Supplementary Material

Efficient photocatalytic methane conversion to oxygenates over TiO2 and Pd co-modified titanium silicalite zeolite

En-Dian Zhao,1,2,[#] Yihong Chen,1,2,[#] Junchi Xu,1 Jun Ma,1,2,* Dong Liu,1,2,*, Yujie Xiong1,2,*

1School of Chemistry and Materials Science, University of Science and Technology of China, Hefei 230026, Anhui, China.

2Sustainable Energy and Environmental Materials Innovation Center, Nano Science and Technology Institute, Suzhou Institute for Advanced Research, University of Science and Technology of China, Suzhou 215123, Jiangsu, China.

[#]The authors contributed equally to this work.

Correspondence to: Prof. Yujie Xiong, Prof. Dong Liu and Dr. Jun Ma, School of Chemistry and Materials Science, University of Science and Technology of China, No.96, Jinzhai Road, Anhui 230026, Hefei, China. E-mails: yjxiong@ustc.edu.cn; dongliu@ustc.edu.cn; junma12@ ustc.edu.cn

Methods

Materials preparation

Preparation of TS@TiO_2:

The titanium silicalite molecular sieve TS-1 was purchased from Jiangsu Xianfeng Nano Material Technology Co., Ltd. (XFF08). Firstly, 0.936 g of TS powder was dispersed into 30 mL of ethanol under stirring. Then, 0.4 mL of tetra-n-butyl titanate (TBOT) and 300 µL of H_2O were dropwise added into the above mixture. After stirring for 4 h, the mixture was transferred into a Teflon-lined autoclave and reacted at 180 °C for 3 h. After that, the white powder was collected through centrifugation, washed three times using ethanol, and dried in an oven. The sample was then annealed at 550 °C for 3 h, which denote as TS@TiO_2. The composite samples with different TiO_2 ratios were synthesized by varying the amount of TBOT[1].

Preparation of SiO_2@TiO_2:

The SiO_2@TiO_2 was synthesized through a sol-gel method. Typically, 1.0 g of SiO_2 spheres with a particle size of about 300 nm were added into a mixed solution containing 79 mL of absolute ethanol, 3.9 mL of concentrated ammonia water, and 1.4 mL of ultrapure water, and ultrasonically dispersed to obtain a colloidal solution of SiO_2. Subsequently, 28 mL of acetonitrile was added into the above colloidal solution in an ice-water bath under stirring. After that, a mixed solution containing 36 mL of absolute ethanol, 12 mL of acetonitrile, and 0.67 mL of TBOT was dropped into the above SiO_2 colloidal solution and kept stirring vigorously for 12 h. Then, the obtained mixture was heated at 110 °C on a plate to evaporate excess solvent. Note that this experiment must be carried out in a fume hood with complete ventilation conditions. Finally, the obtained white powder was annealed at 500 °C for 6 h in a muffle furnace to obtain the SiO2@TiO_2 sample[2].

Preparation of TiO_2 nanoparticles:

Typically, 20 mL of TBOT was mixed with 2.4 mL of hydrochloric acid and stirred for 30 min. Then, the solution was transferred into a 50 mL Teflon-lined autoclave and reacted at 180 °C for 3 h. After that, the resulting white slurry was centrifuged and washed with distilled water several times and dried in a vacuum oven.

Loading of Pd nanoparticles:

The Pd nanoparticles were loaded by the photodeposition method or hydrogen reduction method. Typically, 200 mg of TS@TiO_2 sample was dispersed in 30 mL of water under stirring. Subsequently, 200 μL of K_2PdCl_6 aqueous solution with a concentration of 3.08 mg mL^{-1} was added into the solution and then purged with argon for 30 min to remove oxygen. After stirring for another 10 h, the solution was irradiated under a light intensity of 100 mW cm^{-2} for 30 min. After the photodeposition, the sample was collected by centrifugation, washed three times with water, and dried in a vacuum oven. The obtained samples can be denoted as 0.2Pd-TS@TiO_2. The 0.2Pd-TiO_2 and 0.2Pd-SiO_2@TiO_2 samples were synthesized similarly to 0.2Pd-TS@TiO_2. The 0.2Pd-TS sample was prepared by the hydrogen reduction method. Specifically, 200 mg of TS and 200 μL of K_2PdCl_6 aqueous solution were dispersed in 30 mL of H_2O and stirred for 10 h in the Ar atmosphere. Then the samples were collected by centrifugation and dried in a vacuum oven. The 0.2Pd-TS sample was obtained after annealed at 400 °C for 2 h in a hydrogen atmosphere with a concentration of 5% (argon is the diluent gas).

Etching TS with NaOH solution

Typically, 1 g of TS-1 was added to 50 mL of 0.1 M aqueous sodium hydroxide (NaOH) solution under stirring and heated at 50 °C in an oil bath for 1 h. Then, the sample was filtrated, washed with deionized water, and dried at 80 °C for 24 h to obtain the NaOH-TS. The 0.2Pd-NaOH-TS@TiO_2 was prepared similar to the 0.2Pd-TS@TiO_2.

Materials characterizations

SEM images were taken on a FEI Sirion-200 field emission scanning electron microscope operated at 5 kV. HAADF-STEM images were collected on a Thermo

Scientific Themis Z field-emission transmission electron microscope operated at 300 kV.

Powder XRD patterns were recorded by using a Philips X'Pert Pro Super X-ray diffractometer with Cu-Kα radiation ($\lambda = 1.5418$ Å). UV-vis-NIR diffuse reflectance spectra were recorded in the spectral region of 200-1,500 nm with a Shimadzu SolidSpec-3,700 spectrophotometer.

X-ray photoelectron spectroscopy (XPS) was conducted on Thermo Scientific ESCALAB 250Xi using a monochromatic Al Kα X-ray source.

EPR spectra were collected using a JEOL JES-FA200 electron spin resonance spectrometer at room temperature (9.062 GHz).

Temperature-programmed desorption of CH_4 was carried out on a Micromeritics AutoChem II 2920 apparatus. The 70 mg sample was first pretreated at 200 °C in helium for 1 h and then cooled to room temperature. Subsequently, the sample was saturated in a 10 vol.% CH_4/He atmosphere at 50 °C for 1 h and then flushed with helium flow to remove any physisorbed molecules. Finally, the CO desorption was measured in 30 mL min^{-1} helium flow in the range of 50-700 °C with a heating ramp of 10 °C min^{-1}.

Photocatalytic CH_4 conversion measurement

The customized high-pressure stainless-steel reactor is used to test the photocatalytic methane conversion. Firstly, 10 mg of the catalyst was dispersed in 120 mL of ultrapure water and then transferred into the pressurized stainless steel reactor [Supplementary Figure 24]. After finely sealed, the suspension was purged with ultra-pure oxygen (99.999%) 3 times to completely remove air. Then 1 bar O_2 was maintained in the reactor. Methane (99.999 vol.%) was next injected to acquire the desired pressure. The photocatalytic methane conversion was conducted under ultraviolet light of 365 nm for 2 h. After the reaction, the gaseous products were measured by the gas chromatograph. The CH_3OH and CH_3OOH were analyzed by the 400 MHz liquid superconducting nuclear magnetic resonance spectrometer, while the HCHO was measured through the colorimetric method on the UV-Vis spectrophotometer.

In situ DRIFTS for photochemical CH_4 conversion

In situ DRIFTS measurements were performed using a Bruker IFS 66 v Fourier-transform spectrometer equipped with Harrick diffuse reflectance accessory with ZnSe and quartz window at BL01B in the NSRL in Hefei, China. Each spectrum is recorded by averaging 128 scans at a resolution of 2 cm^{-1}. After sample loading, the pure Ar was purged into the chamber for background spectra collection. Subsequently, the reactant gas was introduced into the chamber. Then, the spectra were collected under dark conditions to record the adsorption process. After that, the system was exposed to light irradiation, and the spectra were collected under light irradiation.

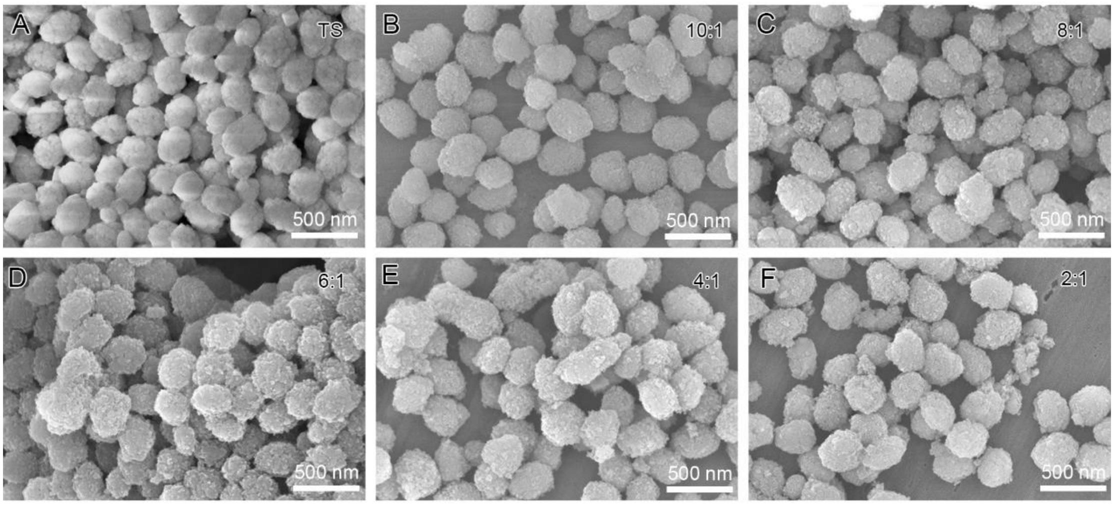

Supplementary Figure 1. SEM images of TS@TiO_2 composite samples with different ratios, (A) TS; (B) TS:TiO_2 = 10:1; (C) TS:TiO_2 = 8:1; (D) TS:TiO_2 = 6:1; (E) TS:TiO_2 = 4:1; (F) TS:TiO_2 = 2:1.

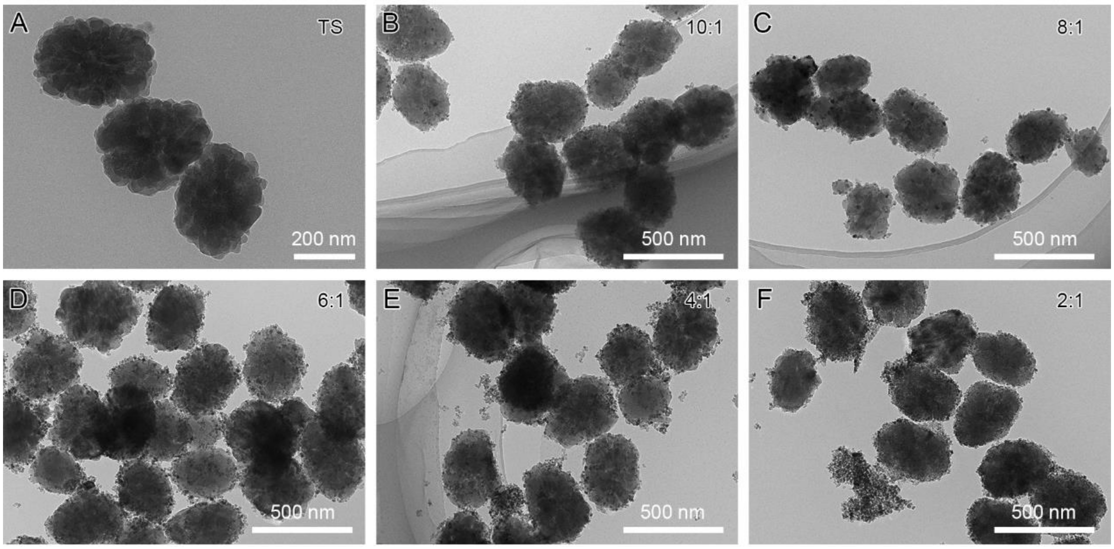

Supplementary Figure 2. TEM images of TS samples and TS@TiO_2 composite samples with different ratios, (A) TS; (B) TS:TiO_2=10:1; (C) TS:TiO_2=8:1; (D) TS:TiO_2=6:1; (E) TS:TiO_2=4:1; (F) TS:TiO_2=2:1.

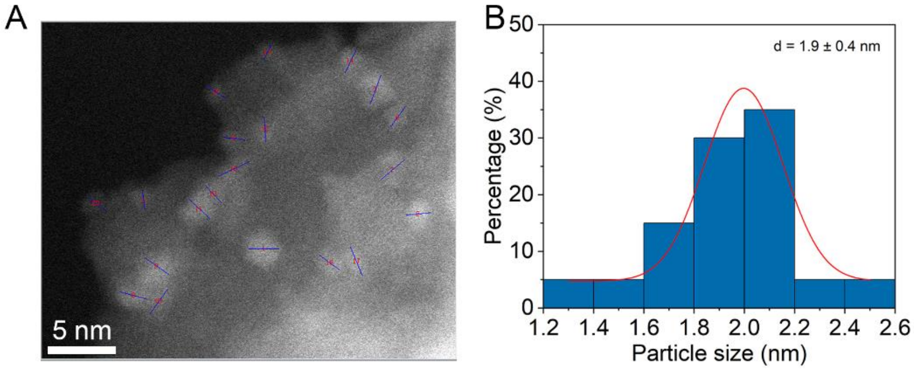

Supplementary Figure 3. (A) HRTEM image and (B) the size distribution of Pd NPs of 0.2Pd-TS@TiO$_2$.

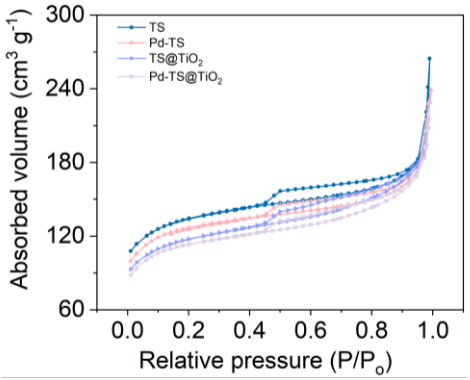

Supplementary Figure 4. Nitrogen sorption isotherms for TS, Pd-TS, TS@TiO$_2$, and Pd-TS@TiO$_2$ samples.

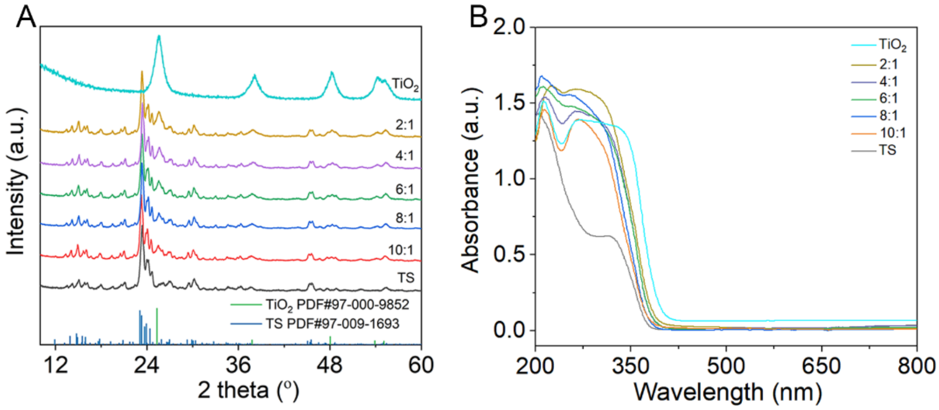

Supplementary Figure 5. (A) XRD patterns and (B) UV-visible diffuse reflectance absorption spectra of TS samples, TiO$_2$ samples, and TS@TiO$_2$ composite samples with different ratios.

As shown in Supplementary Figure 5B**,** the pristine TS sample shows its characteristic absorption. As the increasing of TiO_2 loading, the absorption edge shifts slightly towards longer wavelength. The absorption edge at the wavelength of 218 nm can be attributed to the transition absorption of tetracoordinated titanium in the TS framework. In contrast, the absorption edge at 330 nm is similar to the transition absorption of hexacoordinated titanium in titanium oxide. It is noteworthy that the loading of Pd and TiO_2 on the surface of TS can significantly enhance the light absorption ability of TS, which would definitely improve the performance of photocatalytic reactions.

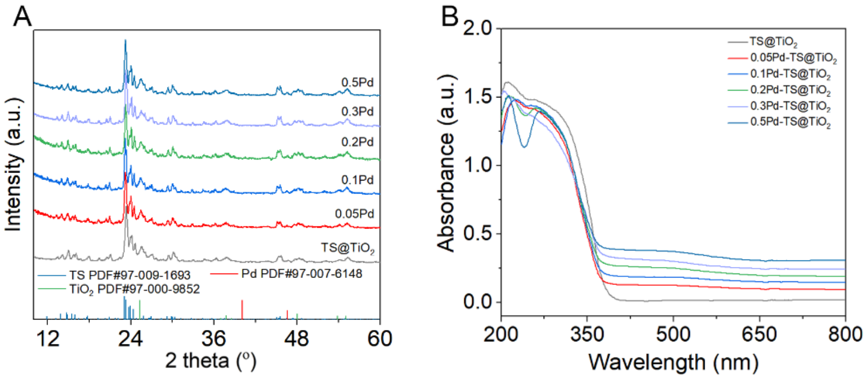

Supplementary Figure 6. (A) XRD patterns and (B) UV-vis diffuse reflectance spectra of different composite samples.

The spectra for all Pd-loaded samples show a noticeable shift at around 220-250 nm compared to the TS@TiO_2. Nevertheless, a slight broadening and more pronounced shift towards higher wavelengths, particularly at around 200-250 nm can be observed as the loading percentage increases. The intensity of the absorbance for 0.1Pd-TS@TiO_2 falls approximately in the middle range among the Pd-doped specimens. Compared to 0.05Pd-TS@TiO_2 and undoped TS@TiO_2, the 0.1Pd-TS@TiO_2 exhibits a higher absorbance intensity at the peak region around 200-250 nm.

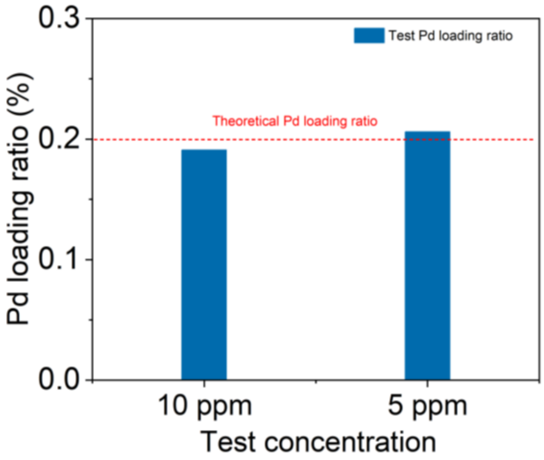

Supplementary Figure 7. The Pd loading ratio detected by ICP-OES.

To ensure the accuracy of the test results, we prepared two solutions with different concentrations (10 ppm and 5 ppm). The test results show that the Pd loading ratios for both concentrations are around 0.2%. This consistency between the two different concentration tests indicates the reliability and accuracy of our measurement method. The two tests suggest that the Pd loading ratio on our material is indeed around 0.2%, regardless of the test concentration.

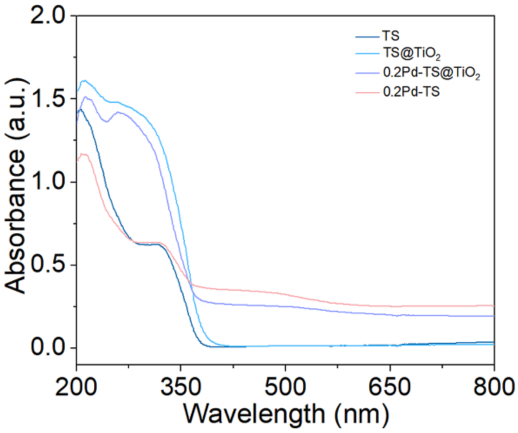

Supplementary Figure 8. Ultraviolet-visible diffuse reflectance spectra of TS, 0.2Pd-TS, TS@TiO_2, and 0.2Pd-TS@TiO_2 samples.

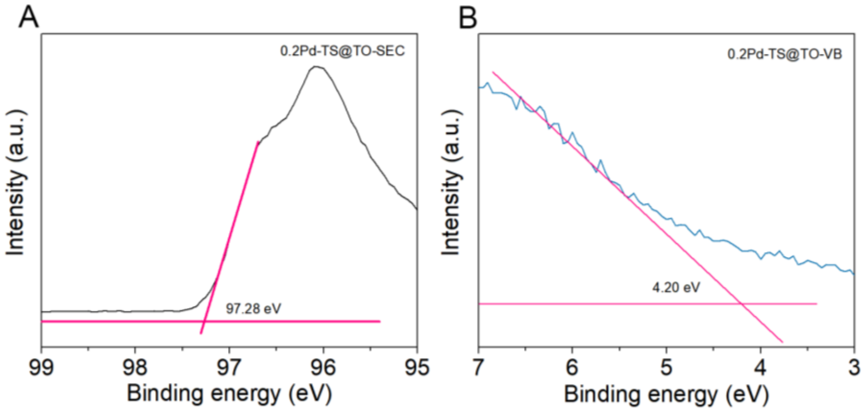

Supplementary Figure 9. (A) Secondary electron cutoff and (B) valence band spectra of 0.2Pd-TS@TiO$_2$ sample.

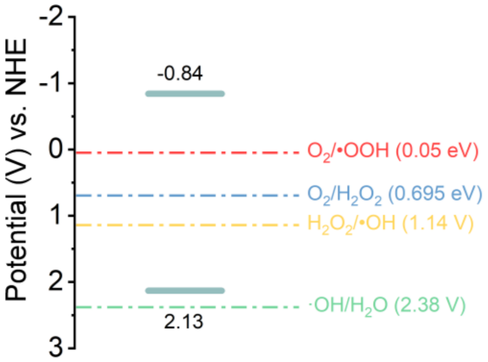

Supplementary Figure 10. Illustration for the band structure of 0.2Pd-TS@TiO$_2$.

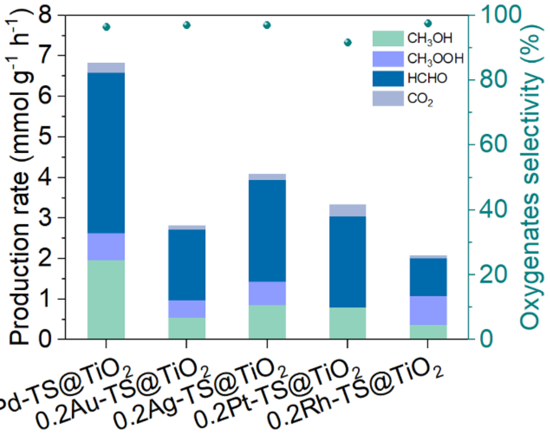

Supplementary Figure 11. Photocatalytic methane conversion performance over 0.2Pd-TS@TiO$_2$, 0.2Au-TS@TiO$_2$, 0.2Ag-TS@TiO$_2$, 0.2Pt-TS@TiO$_2$, and 0.2Rh-TS@TiO$_2$ samples.

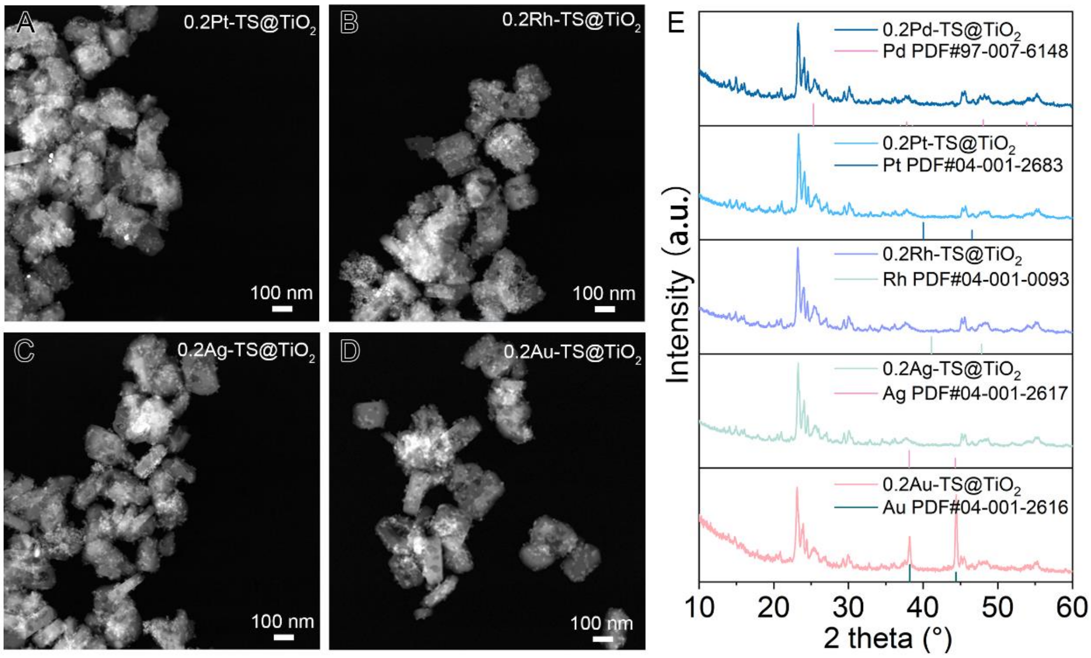

Supplementary Figure 12. (A-D) TEM images and (E) XRD patterns of 0.2Pt-TS@TiO$_2$, 0.2Rh-TS@TiO$_2$, 0.2Ag-TS@TiO$_2$, 0.2Au-TS@TiO$_2$ and 0.2Pd-TS@TiO$_2$.

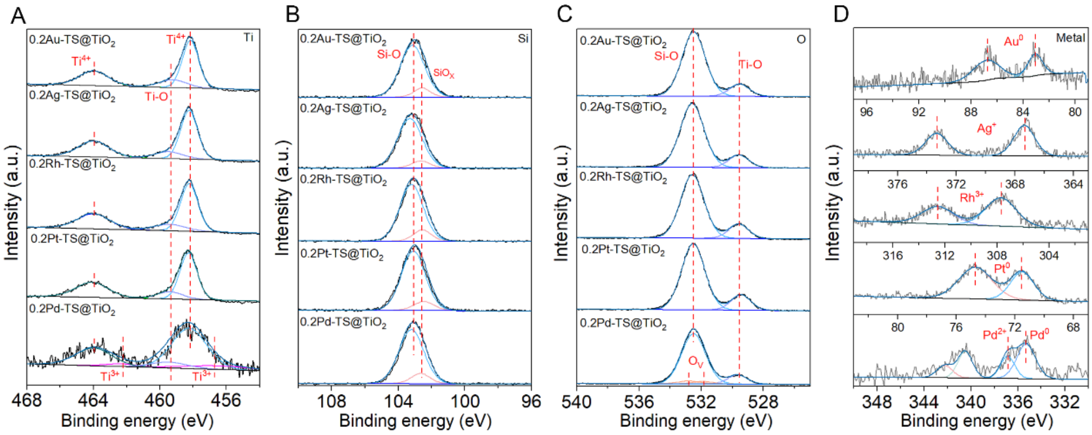

Supplementary Figure 13. (A)Ti 2p, (B) Si 2p, (C) Pd 3d and (D) O 1s XPS spectra of 0.2Au-TS@TiO$_2$, 0.2Ag-TS@TiO$_2$, 0.2Rh-TS@TiO$_2$, 0.2Pt-TS@TiO$_2$, 0.2Pd-TS@TiO$_2$.

According to the Ti XPS spectra [Supplementary Figure 13A], it is obvious that a distinct Ti^{3+} peak appears upon the incorporation of Pd into TS@TiO$_2$. This result suggests that the introduction of Pd leads to the partial reduction of Ti^{4+} to Ti^{3+}, which is often associated with the formation of oxygen vacancies [Supplementary Figure 14A]. However, the oxygen vacancy can hardly be detected on other metals (such as Au, Ag, Pt, Rh) loaded on TS@TiO$_2$ catalysts [Supplementary Figure 14B], indicating relatively weaker interactions between these metals and TS@TiO$_2$.

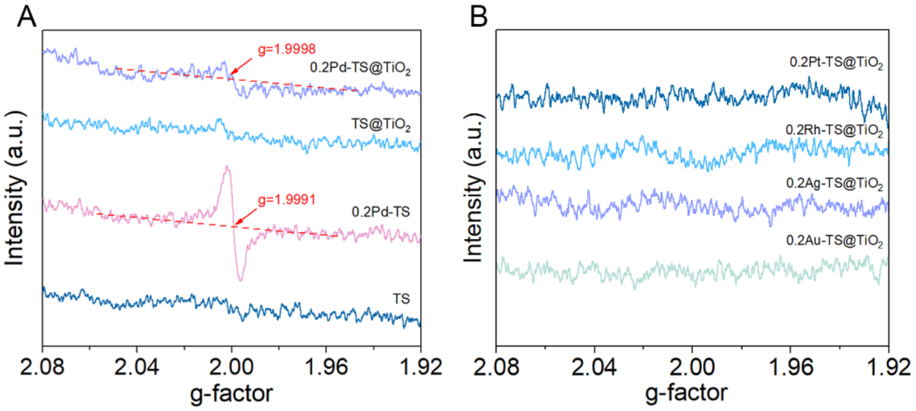

Supplementary Figure 14. (A) EPR spectra of TS, 0.2Pd-TS, TS@TiO$_2$, and 0.2Pd-TS@TiO$_2$; (B) EPR spectra of 0.2Au-TS@TiO$_2$, 0.2Ag-TS@TiO$_2$, 0.2Rh-TS@TiO$_2$, 0.2Pt-TS@TiO$_2$ samples.

Compared to the TS and TS@TiO$_2$ samples, the 0.2Pd-TS and 0.2Pd-TS@TiO$_2$ samples, with added Pd, display more pronounced EPR signal peaks. This demonstrates that the introduction of the Pd element indeed leads to the appearance of oxygen defects. In the samples without added Pd (TS and TS@TiO$_2$), the oxygen vacancy EPR signal are hardly detected, which is consistent with the XPS in Figure 2.

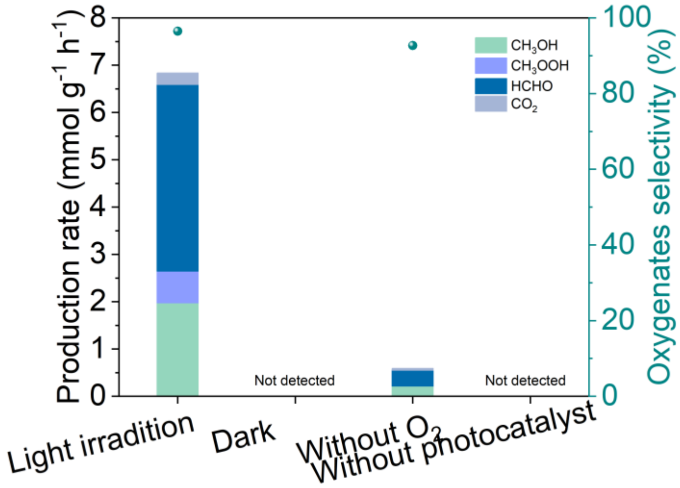

Supplementary Figure 15. The control experiments of photochemical CH_4 conversion over 0.2Pd-TS@TiO_2.

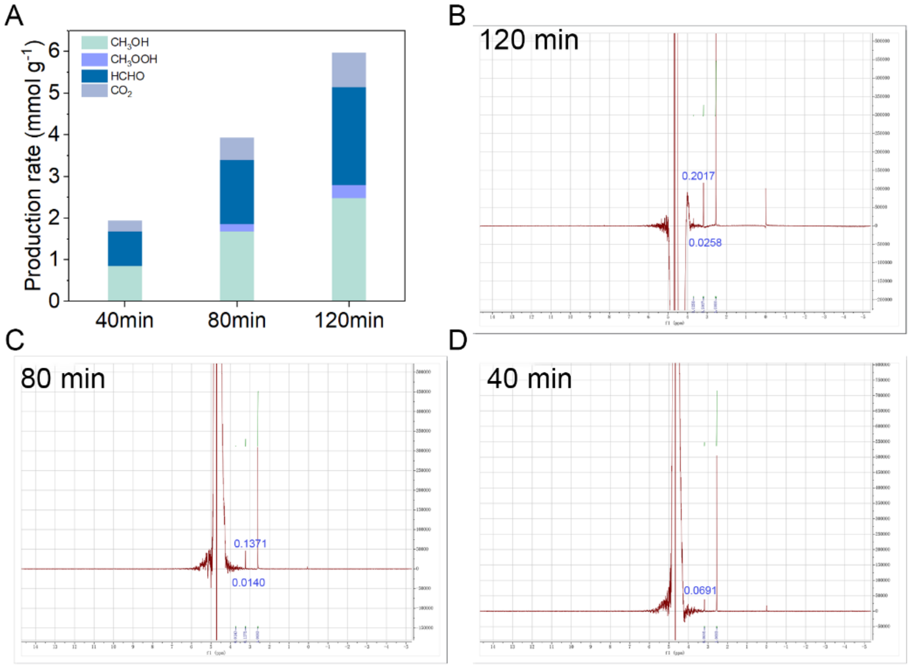

Supplementary Figure 16. (A) The production rate of the products at different reaction times. (B-D) The 1H NMR spectra of the reaction solution after different reaction times.

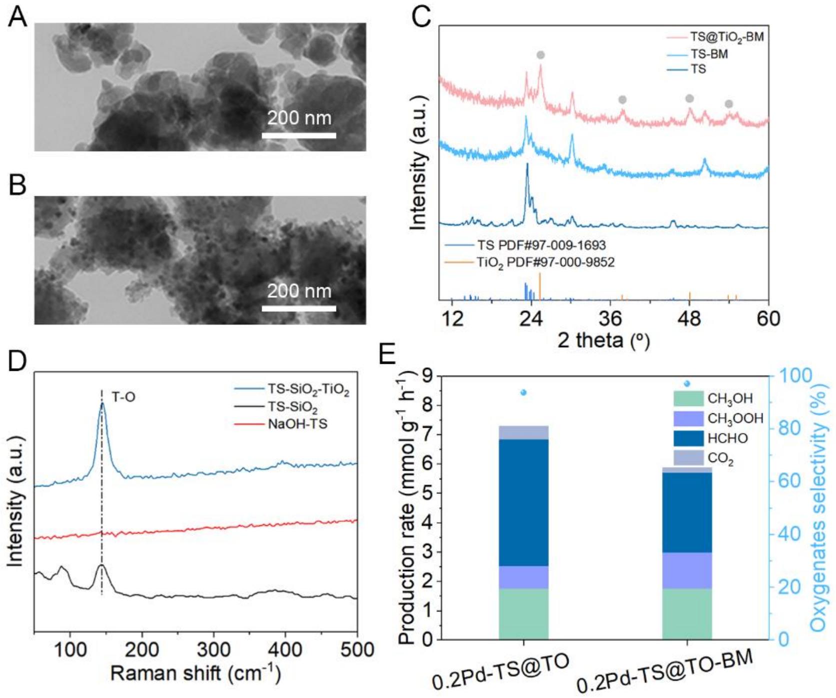

Supplementary Figure 17. TEM images of (A)TS-BM and (B) TS@TiO_2-BM samples; (C) XRD diffraction patterns and (D) Raman spectra of TS, TS-BM and TS@TiO_2-BM samples; (E) Photocatalytic oxygen-containing conversion performance of methane of 0.2Pd-TS@TiO_2-BM and 0.2Pd-TS@TiO_2-BM samples.

The porous structure of TS was destroyed by ball milling (marked as TS@TiO_2-BM). Then, titanium oxide particles were grown on its surface by the same solvothermal method (marked as TS@TiO_2-BM). The XRD characterization results showed that the molecular sieve crystal phase structure of the TS-BM and TS@TiO_2-BM samples had been damaged. At the same time, the TS@TiO_2-BM sample also showed obvious diffraction peaks of anatase TiO_2 (Supplementary Figure 17C, the diffraction peak marked by the gray solid dot), indicating that titanium oxide particles were successfully modified on the surface of the TS@TiO_2-BM sample. Raman spectroscopy indicated [Supplementary Figure 17D] that there was originally a signal at 145 cm^{-1} on the TS surface, which could be attributed to the Ti-O bond in a structure similar to anatase TiO_2. This signal did not appear in the treated TS-BM sample, indicating that the Ti-O site similar to anatase TiO_2 on the TS surface had been damaged or changed. In addition, the TS@TiO_2-BM sample had a strong Raman signal at 145 cm^{-1}, which further verified the existence of titanium oxide particles. Subsequently, Pd particles were loaded on the TS@TiO_2-BM sample and the photocatalytic oxygen-containing conversion performance test of methane was carried out on this sample.

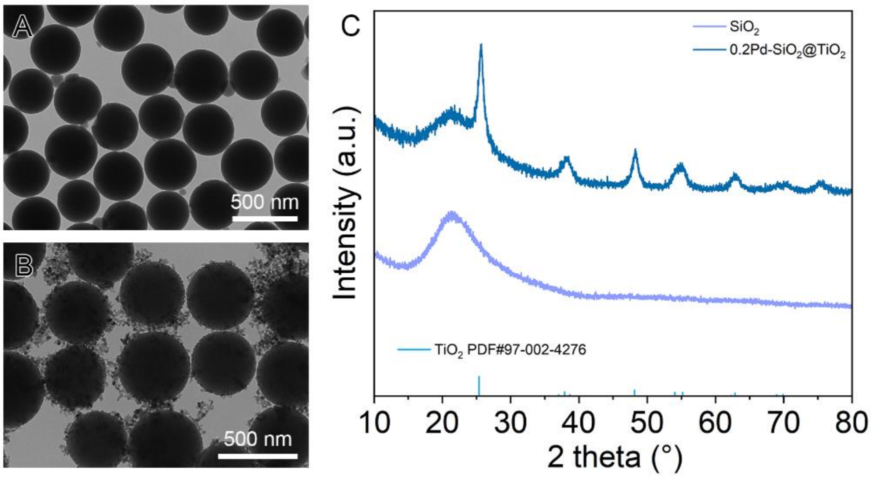

Supplementary Figure 18. TEM images of (A) SiO_2 and (B) 0.2Pd-SiO_2@TiO_2 samples; (C) XRD patterns of SiO_2 and 0.2Pd-SiO_2@TiO_2 samples.

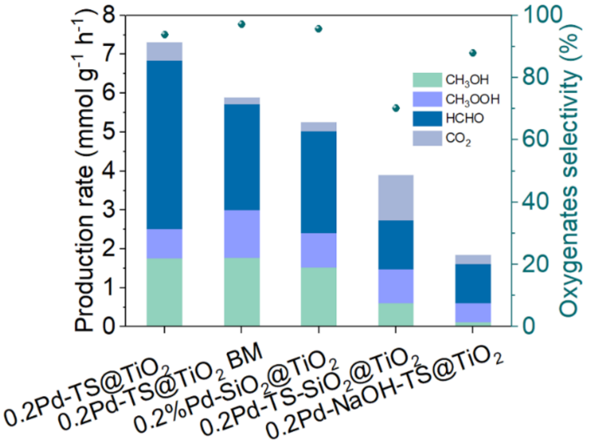

Supplementary Figure 19. Photocatalytic methane conversion performance over 0.2Pd-TS@TiO_2, 0.2Pd-TS@TiO_2-BM, 0.2Pd-SO@TiO_2, 0.2Pd-TS-SO@TiO_2, 0.2Pd-NaOH-TS@TiO_2 samples.

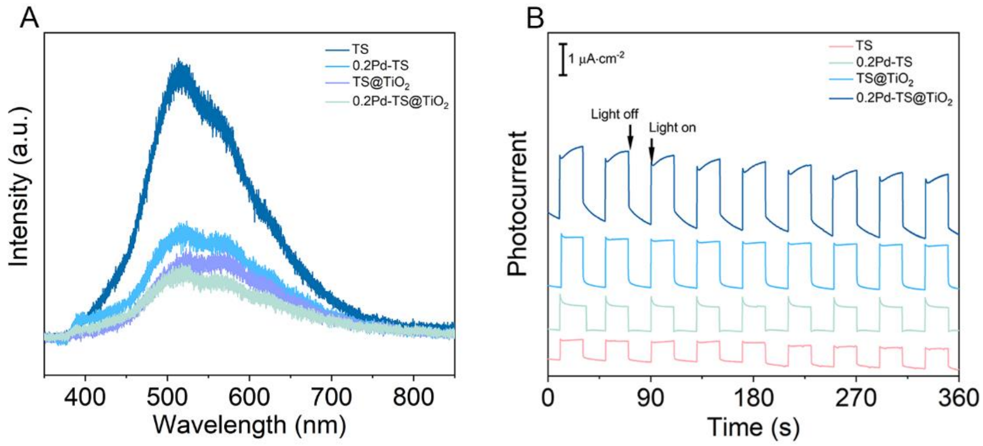

Supplementary Figure 20. (A) Photoluminescence spectrum with an excitation wavelength of 320 nm. (B) Photocurrent response in a CH_4 atmosphere, with an applied bias voltage of 0.8 V *vs.* Ag/AgCl.

As shown in Supplementary Figure 20, the 0.2Pd-TS@TiO_2 exhibits much weaker photoluminescence intensity, indicating lower photogenerated carrier recombination and efficient photogenerated carrier separation. Moreover, the 0.2Pd-TS@TiO_2 catalyst exhibits the highest photocurrent response in the CH_4 atmosphere, further suggesting the improved photogenerated charge carrier transfer efficiency. Note that the electrochemical characterization was conducted in the CH_4-saturated electrolyte to evaluate the photogenerated carrier separation for CH_4 conversion.

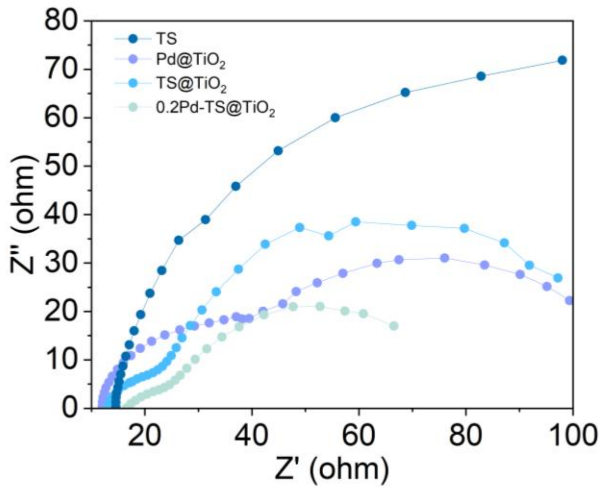

Supplementary Figure 21. Electrochemical impedance spectroscopy (EIS) spectrum of TS, Pd@TiO_2, TS@TiO_2, 0.2Pd-TS@TiO_2.

As shown in Supplementary Figure 21, the 0.2Pd-TS@TiO_2 presents the lowest impedance, indicating the efficient electron transport upon Pd and TiO_2 loading. The synergistic effect of both Pd and TiO_2 significantly lowers the electron transport resistance, resulting in superior photocatalytic performance for methane oxidation.

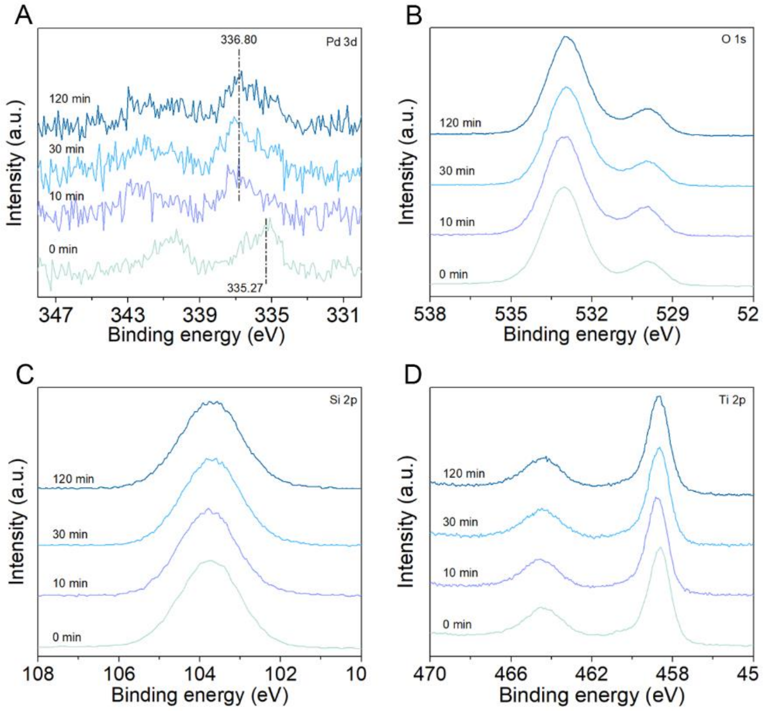

Supplementary Figure 22. (A) Pd 3d; (B) O 1s; (C) Si 2p; and (D) Ti 2p XPS spectra of 0.2Pd-TS@TiO_2 sample under light irradiation.

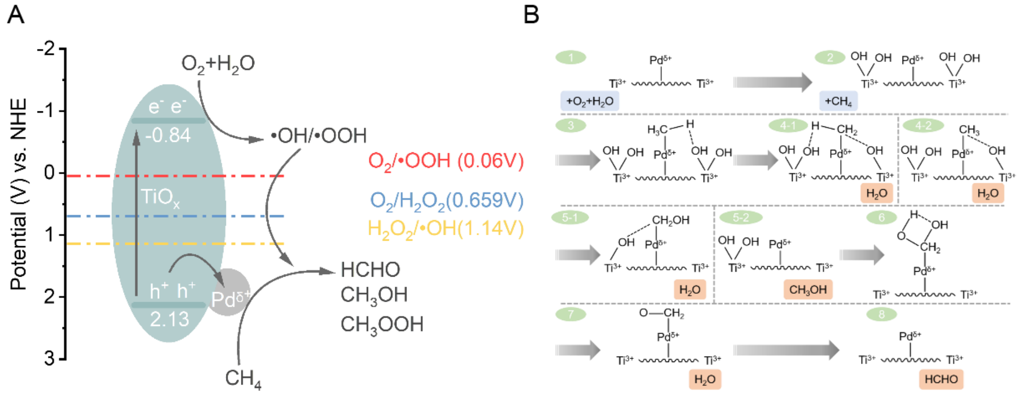

Supplementary Figure 23. (A) Schematic diagram of the band structure of 0.2Pd-TS@TiO_2 sample and photocatalytic CH_4 conversion process; (B) Schematic diagram of the reaction pathways for photocatalytic CH_4 conversion over 0.2Pd-TS@TiO_2 sample.

The main reaction equation:

(1) Pd-TS@$TiO_2 \xrightarrow{hv\ (light)} h^+ + e^-$

(2) $H_2O + h^+ \longrightarrow \cdot OH + H^+$

(3) $CH_4 + \cdot OH \longrightarrow {}^*CH_3 + H_2O$

(4) ${}^*CH_3 + \cdot OH \longrightarrow CH_3OH$

(5) $CH_3OH + 2OH \longrightarrow HCHO + 2H_2O$

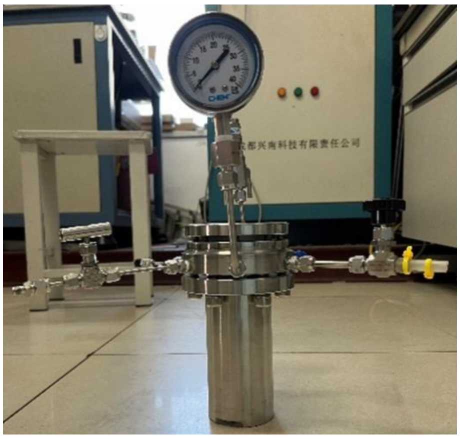

Supplementary Figure 24. The optical image of the high-pressure stainless-steel reactor.

Supplementary Table 1. The surface area and pore structure parameters of different samples

Sample name	Surface area (m^2 g^{-1})	Pore volume (m^3 g^{-1})	Pore diameter (nm)
TS	430.84	0.25	2.62

0.2Pd-TS	406.62	0.22	2.69
TS@TiO_2	379.05	0.22	2.92
0.2Pd-TS@TiO_2	364.43	0.22	2.92

Supplementary Table 2. Representative works on light-driven CH_4 conversion under mild conditions

Samples	**Product**	**Production rate**	**Selectivity**	**Reference**
0.2Pd-TS@TO	Oxygenate products	6800 μmol gcat.$^{-1}$ h^{-1}	96.5%	This work
Pd1/TS-1@CN	Oxygenate products	647 μmol gcat.$^{-1}$ h^{-1}	100%	[3]
Pd9Au1NWs/Z-5	Oxygenate products	11570 μmol gcat.$^{-1}$ h^{-1}	95.1%	[4]
Cu-0.5/PCN	CH_3CH_2OH	106 μmol gcat.$^{-1}$ h^{-1}	81.2%	[5]
ZnO/Fe_2O_3	CH_3OH	118.84 μmol gcat.$^{-1}$ h^{-1}	99.6%	[6]
La-WO_3	CH_3OH	36.7 μmol gcat.$^{-1}$ h^{-1}	46%	[7]
PdO/Pd-WO_3	CH_3COOH	1500 μmol gPd^{-1} h^{-1}	91.6%	[8]
Cu-def-WO_3	HCHO	2489 μmol gcat.$^{-1}$ h^{-1}	100%	[9]
$CsPbBr_3$/$BiVO_4$	Oxygenate products	533.5 μmol gcat.$^{-1}$ h^{-1}	94.8%	[10]

SUPPLEMENTARY REFERENCES

1. Shi, Y.; Zhou, Y.; Lou, Y.; Chen, Z.; Xiong, H.; Zhu, Y. Homogeneity of

Supported Single-Atom Active Sites Boosting the Selective Catalytic Transformations. *Adv. Sci.* **2022**, *9*, 2201520, doi:10.1002/advs.202201520.

2. Sun, Y.; Li, G.; Gong, Y.; Sun, Z.; Yao, H.; Zhou, X. Ag and TiO2 nanoparticles co-modified defective zeolite TS-1 for improved photocatalytic CO2 reduction. *J. Hazard. Mater.* **2021**, *403*, 124019, doi:10.1016/j.jhazmat.2020.124019.
3. Yu, B.; Cheng, L.; Wu, J.; Yang, B.; Li, H.; Xu, J.; Zhang, Y.; Pan, C.; Cao, X.-M.; Zhu, Y.; Lou, Y. Surface hydroxyl group dominating aerobic oxidation of methane below room temperature. *Energy Environ. Sci.* **2024**, *17*, 8127-8139, doi:10.1039/d4ee03508a.
4. Tan, L.; Shi, Y.; Xu, Y.; Zhang, X.; Wu, D.; Wang, Z.; Xiao, J.; Wen, H.; Li, J.; Tian, X.; Deng, P. Ultrathin PdAu Nanowires with High Alloying Degree for the Direct Oxidation of Methane to C1 Oxygenates. *Chin. J. Chem.* **2024**, *42*, 2999-3005, doi:10.1002/cjoc.202400591.
5. Zhou, Y.; Zhang, L.; Wang, W. Direct functionalization of methane into ethanol over copper modified polymeric carbon nitride via photocatalysis. *Nat. Commun.* **2019**, *10*, 506, doi:10.1038/s41467-019-08454-0.
6. Zheng, K.; Wu, Y.; Zhu, J.; Wu, M.; Jiao, X.; Li, L.; Wang, S.; Fan, M.; Hu, J.; Yan, W.; et al. Room-Temperature Photooxidation of CH4 to CH3OH with Nearly 100% Selectivity over Hetero-ZnO/Fe2O3 Porous Nanosheets. *J. Am. Chem. Soc.* **2022**, *144*, 12357-12366, doi:10.1021/jacs.2c03866.
7. Villa, K.; Murcia-López, S.; Morante, J.R.; Andreu, T. An insight on the role of La in mesoporous WO3 for the photocatalytic conversion of methane into methanol. *Appl. Catal. B-Environ.* **2016**, *187*, 30-36, doi:10.1016/j.apcatb.2016.01.032.
8. Zhang, W.; Xi, D.; Chen, Y.; Chen, A.; Jiang, Y.; Liu, H.; Zhou, Z.; Zhang, H.; Liu, Z.; Long, R.; Xiong, Y. Light-driven flow synthesis of acetic acid from methane with chemical looping. *Nat. Commun.* **2023**, *14*, 3047, doi:10.1038/s41467-023-38731-y.
9. Luo, L.; Han, X.; Wang, K.; Xu, Y.; Xiong, L.; Ma, J.; Guo, Z.; Tang, J. Nearly 100% selective and visible-light-driven methane conversion to formaldehyde via. single-atom Cu and Wδ+. *Nat. Commun.* **2023**, *14*, 2690, doi:10.1038/s41467-023-

38334-7.

10. Dong, G.-X.; Zhang, M.-R.; Su, K.; Liu, Z.-L.; Zhang, M.; Lu, T.-B. Visible-light-driven and selective methane conversion to oxygenates with air on a halide-perovskite-based photocatalyst under mild conditions. *J. Mater. Chem. A* **2023**, *11*, 9989-9999, doi:10.1039/d3ta01405c.